Enabling Manufacturable Optical Broadband Angular-Range Selective Films

Enabling Manufacturable Optical Broadband Angular-Range Selective Films

Kezhen Yin[1*†], Yurui Qu[2†], Steven E. Kooi [3], Wei Li[1], Jingxing Feng[4], Jo Ann Ratto[5], John D. Joannopoulos[6], Marin Soljačić[6], Yichen Shen[1, 6*]

[1]Lux Labs, Inc. Boston, MA 02210, USA

[2]Department of Electrical and Computer Engineering, University of Wisconsin-Madison, Madison, WI 53706, USA

[3]Institute for Soldier Nanotechnologies, Massachusetts Institute of Technology, Cambridge, MA 02139, USA

[4]Department of Macromolecular Science and Engineer, Case Western Reserve University, Cleveland, OH 44106, USA

[5]Soldier Protection Directorate, U.S. Army Combat Capabilities Development Command Soldier Center (DEVCOM SC), Natick MA 01760 USA

[6]Department of Physics, Massachusetts Institute of Technology, Cambridge, MA 02139, USA

[†]These authors contributed equally to this work

*email: kezhen@luxlabs.co; yichen@luxlabs.co

ABSTRACT:

The ability to control the propagation direction of light has long been a scientific goal. However, the fabrication of large-scale optical angular-range selective films is still a challenge. This paper presents a polymer-enabled large-scale fabrication method for broadband angular-range selective films that perform over the entire visible spectrum. Our approach involves stacking together multiple one-dimensional photonic crystals with various engineered periodicities to enlarge the band gap across a wide spectral range based on theoretical predictions. Experimental results demonstrate that our method can achieve broadband transparency at a range of incident angles centered around normal incidence and reflectivity at larger viewing angles, doing so at large scale and low cost.

KEYWARDS: polymer, multilayer, optical film, angular selective, broadband.

An electromagnetic plane wave is characterized by three fundamental properties: the frequency, the polarization, and the propagation direction. Tremendous progress has been made toward achieving both frequency and polarization selectivity. Angular selectivity, however, has seen relatively slower progress over the past several decades. Some studies have explored angular selectivity based on metamaterials [1-2] and photonic crystals; [3-4] however, these methods can only achieve narrowband angular selectivity due to their inherent resonant properties. Some progress has been made toward achieving optical broadband angular selectivity, including methods based on

extraordinary transmission, [5-6] a combination of polarizers and birefringent films, [7] or parabolic directors. [8] The first method is difficult to realize in the visible spectrum; while the other two can only work as angularly selective absorbers.

One major application for broadband angular-range selective films is in solar energy harvesting, such as in solar cells. [9-11] A broadband angularly selective film can help mitigate emission losses from radiative recombination and incomplete absorption, through the process of photon-recycling and light trapping. [12] Privacy screens are the other major application, and can be widely used in mobile phones and computer displays. [13-14] Other applications include detectors with enhanced signal-to-noise ratios, [12] car window privacy and sun shields. Practical applications require large-scale production and low cost, and therefore it is important to achieve manufacturable optical films with broadband angular-range selectivity. Shen *et al*.; [15] proposed that one can utilize the Brewster angle of two isotropic dielectric media to achieve broadband angular selectivity however, the film only works when it is immersed in an index-matching liquid and such a method cannot be used for large-scale film production and implementation. Some theoretical studies have demonstrated that one-dimensional photonic crystal (1D PhC) structures based on anisotropic and isotropic bilayers can achieve optical broadband angular selectivity, [16-17] but experimental demonstrations are still lacking. So far, producing broadband angularly selective films at a large-scale and low cost has remained elusive.

In this paper, we demonstrate the concept of polymer-enabled manufacturable optical broadband angular-range selective films. First, we theoretically prove the

concept of angular-range selectivity over the entire visible spectrum based on 1D PhCs consisting of alternating anisotropic and isotropic layers. The use of anisotropic material is absolutely key in this regard. Second, we use the guidance provided by the theoretical results to design and fabricate an optical angularly selective film based on two commercial polymers, polyamide and polyester, *via* an industrial multilayer co-extrusion technique followed by an orientation process. The experimentally measured angular-range selective film exhibits, over the entire visible spectrum, high transmissivity (~80%) at a range of angles centered at normal incidence, and high reflection (~75%) at incident angles at and above 60°. This range of selectivity is appropriate for the variety of applications mentioned above, and the fabrication approach is large-scale and low cost.

RESULTS AND DISCUSSION

We first show the fundamental physical principle of broadband angular-range selectivity. Consider a one-dimensional photonic crystal (1D PhC) consisting of alternating anisotropic layers (A) with refractive indices $n_A = (n_{xx}^A, n_{yy}^A, n_{zz}^A)$ = (1.57, 1.53, 1.51) and isotropic layers (B) with refractive index n_B = 1.57, as shown in Fig. 1a. As we shall see in section 3, these values correspond to accessible material choices. For simplicity, we only focus on *p*-polarized light in the x direction. We note that such a material system can further be generalized to include both s and p polarizations. [16] The analytical expressions for the effective refractive index n_A^p of the anisotropic layer (A) for p_x-polarized light at a specific incident angle is given as follows: [17]

$$n_A^p = \frac{1}{\sqrt{\frac{cos^2\theta_A^p}{\mu_{yy}n_{xx}^2/\mu_0\varepsilon_0} + \frac{sin^2\theta_A^p}{\mu_{yy}n_{zz}^2/\mu_0\varepsilon_0}}} . \quad (1)$$

In this work, the permeability μ of material A and B is 1. θ_A^p is the refraction angle for p_x-polarized light in layer A. From equation (1), we see that the refractive index of the anisotropic layer is affected by n_{zz}. For near normal incidence, $\sin\theta_A^p \approx 0$, n_A^p increases slightly with increasing anisotropy, therefore p_x-polarized light "sees" almost the same refractive index of material A and B and is totally transmitted (black line in Fig. 1b). However, for incidence angles not close to normal, n_A^p increases more rapidly with increasing anisotropy. Large anisotropy in permittivity results in high index contrast and band gaps opening up at select wavelengths related to those angles (see example for 30^0, 45^0, 60^0 incidence angles in Fig. 1b). Here there are 80 anisotropic- isotropic bilayers in 1D PhC and the period is 100 nm. The simulation is based on the rigorous coupled wave analysis (RCWA). [18]

To cover the entire visible spectrum, 1D PhC layers with various periodicities are stacked together to enlarge the collective band gap (see Fig. 1c). The location of the band gap scales proportionally with the periodicity of the multilayer stack, and therefore the effective band gap can be enlarged when we stack multilayer stacks with various periodicities together. As a proof of principle, we plot the transmission spectra of a multilayer structure consisting of 85 such stacks, each stack consisting of 50 isotropic-anisotropic bilayers (see Fig. 1d). The period of the *i*th stack (i = 1, 2, . . . , 85) should be $1.01^{(i-1)}a_1$, where a_1 is the period of the first stack facing the incident light (a_1=65 nm). The isotropic and anisotropic materials have refractive indices of n_A=1.57 and n_B= (1.57, 1.53, 1.51), respectively. The thickness ratio between layer A and B is 1:1. By

doing this, we can achieve angular-range selectivity with broad bandwidth (400 to 700 nm) and finite angular range (0° to 45°). To demonstrate that the anisotropic layer is the key to achieve angular-range selectivity, we calculate the transmission spectrum of a multilayer structure with two isotropic materials with refractive indices n_A=1.57 and n_B= 1.51. The multilayer structure behaves like a mirror for all incident angles (Fig. 1e). The multilayer structure consists of 1000 stacks, each stack consisting of 50 isotropic-anisotropic bilayers. The period of the *i*th stack is $1.001^{(i-1)}a_1$ where a_1 equals 65 nm. Practical manufacturing conditions will often require off-ratio structures for production feasibility. For example, the thickness ratio between layers A and B is often not 1:1, but 1:2 or 1:3 in realistic manufacturing conditions. Here we calculate the transmission spectrum of the multilayer structure with the thickness ratio between layer A and B is 1:3. We can see that the transparent angular range increases to 0°-55° (Fig. 1f).

In realistic manufacturing conditions, layer distribution in the multilayer structure may not be as perfect as expected. Next, we show that random distribution of multilayer stacks with various periodicities can also result in broadband angular-range selectivity. First, we plot transmission spectra of a multilayer structure consisting of 30 stacks with sequential distribution (Fig. 2a). Each stack consisting of 100 isotropic-anisotropic bilayers. The refractive indices of isotropic layers (A) and anisotropic layers (B) are is n_A = 1.57 and n_B = (1.57, 1.53, 1.51), respectively. The period of the *i*th stack (i = 1, 2, . . . , 30) should be a_1+(i-1)×3nm, where a_1 equals 70 nm (Fig. 2b). The thickness ratio between layer A and B is 1:1. Angular-range selectivity with broad bandwidth (400 to 700 nm) and finite angular range (0° to 60°) is achieved. The random

permutation of these multilayer stacks with various periodicities is implemented (Fig. 2d). The broadband angular-range selectivity can still be achieved and the performance is as good as that of the sequentially distributed multilayer structure (Fig. 2c). This gives much flexibility for the manufacture of hundred-layer-films with no need for careful arrangement of each stack.

To demonstrate optical broadband angular-range selective film production within a practical large-scale manufacturing approach requires overcoming several critical bottlenecks. First, use of inorganic semiconductors/insulators is prohibitive from the point of view of scale and cost. Polymer based structures are more promising and offer a range of lab-scale production techniques, including chemical vapor deposition, layer-by-layer coating, and self-assembly. While these techniques are all capable of producing multilayer films, they suffer from low processing speed, high cost, and small film size for the manufacture of hundred-layer-films. On the other hand, a multilayer co-extrusion approach represents an advanced processing technique capable of producing polymer films with thousands of layers economically and effectively. [19] However, in order to achieve layer configurations with the desired architecture, material selection and processing-parameter control are essential for matching viscosity and elasticity of the polymer melt during extrusion. Additionally, a sophisticated design involving multi-layer feed-block with hundreds of polymer flow channels is necessary to generate uniform layer structures. Secondly, one needs to deal with the anisotropic/isotropic bilayer structure which is, in general, difficult to design and manufacture. Nevertheless, an anisotropic layer can be obtained *via* polymer orientation

(induced by post extrusion stretching) with a few candidates including polyethylene (PE), polypropylene (PP), polyester (PET), polyamide (PA), polystyrene (PS), and polyvinylidenefluoride (PVDF). Each material requires its own specific stretching condition to achieve the desired orientation. Therefore, the processing window is especially narrow for multilayer films where the orientation properties of both materials is critical. Moreover, the particular stretching parameters needed to generate orientation for the anisotropic layer while keeping the other layer isotropic are quite complex. Last but not least, the angular-range selective film must possess the desired optical properties. The refractive indices (n) must match in the in-plane x direction in both layers for normal direction transparency while the refractive indices must differ (Δn) in the out-of-plane direction (z-direction) of both layers for the angle dependent bandgap. Given these mechanical and optical constraints we found 2 polymers, polyamide (PA) and polyethylene terephthalate glycol (PETG), that are most appropriate. PA is chosen as the anisotropic material since it possesses a wide stretching window and matches the in-plane index of PETG, and PETG is chosen as the isotropic material since amorphous PETG remains amorphous (isotropic) under the appropriate processing conditions during the post-extrusion stretching of the film. In this work we use this approach to demonstrate a large scale, fast speed, and low-cost manufacturing technique to produce material systems that possess optical broadband angular-range selectivity. It should be emphasized that the method in this paper is not based on any lab scale equipment and process. The films were produced *via* industry pilot scale equipment with a through put of 100lbs./hr. The as-extruded film we collected is in 100 ft roll with 12 i width. The

final angular selective film is able to cover a cell phone screen which exhibits large scale angular selectivity effect.

Specifically, 1D PhC films with alternating PA anisotropic layers (A) and PETG isotropic layers (B) were fabricated *via* the multilayer co-extrusion technique (Fig. 3a) followed by a post-extrusion orientation step. Each individual 1D PhC film consists 121 anisotropic layers ($n^p_{A,xx} = 1.57,\ n^p_{A,yy} = 1.53,\ n^p_{A,zz} = 1.51$) and 120 isotropic layers ($n^p_{B,xx} = n^p_{B,yy} = n^p_{B,zz} = 1.57$) with a layered structure that was confirmed by atomic force microscopy (Fig. 3b). The refractive indices of PA layer were obtained by measuring the PA control film with the same processing condition and the refractive indices of PETG were selected from isotropic PETG film. The film is totally transmissive ($n^p_A = n^p_B$) for p_x-polarized light at normal incidence (black line in Fig. 3c), whereas, a band gap is exhibited ($n^p_A < n^p_B$) for p_x-polarized light with an incident angle of 60° (red line in Fig. 3c).

To cover the entire visible spectrum, an angular-range selective film was produced by stacking together 20 of the 1D PhC stacks, each with distinct periodicities. Each stack consists of 241 anisotropic-isotropic bilayers. The thickness ratio between isotropic layer and anisotropic layer is 1:3. The thickness of the isotropic layer in the *i*th (i = 1, 2, …20) stack should be a_1+[(i-1)/2] × 3nm, where a_1 equals 45 nm. The thickness of the anisotropic layer in each stack is triple that of the isotropic layer. The fabricated angular-range selective film exhibits around 80% transmissivity (black line in Fig. 3d) for p_x-polarized light at normal incidence, whereas, the p_x-polarization light transmissivity is decreased to around 25% at an incident angle of 60° (red line in Fig. 3d).

In Fig. 4, we calculate the p_x-polarization transmittance of the sample and measure the corresponding experimental transmittance in the visible spectrum. First, we calculate the p_x-polarization transmittance in ideal case. The sample shows high transparency (~100%) for normal incidence (Fig. 4a). The transmittance of the sample remains larger than 90% when the incident angle is smaller than 30° and starts to decrease when the incident angle is further increased. The multilayer structure becomes reflective and behaves like mirror when the angle is larger than 60°. Given that the small nonuniformity that exist in the layers of the fabricated material can reduce transparency, the transmission spectrum is then calculated including a scattering correction to make theoretical and experimental spectra for normal incidence agree with each other. Specifically, the correction involves taking the ratio of transmission data at normal incidence for the experimental and ideal simulations as the correction factor applied across the entire spectrum. The corrected transmittance still shows high transparency (~80%) for normal incidence (Fig. 4b). When the incident angle is increased to 60°, the multilayer structure becomes highly reflective and behaves like mirror. The transmittance of the sample was measured using an ultraviolet-visible spectrophotometer (Ocean Optics SD 2000). The sample shows high transparency (~80%) for normal incidence and highly reflection at the incident angle of 60° in the experiment. The experimental transmittance agrees reasonably well with the calculated results (Fig. 4c).

In order to demonstrate the performance of the angular-range selective film, it is placed in front of an iPhone whose display is a set to a rainbow image, as shown in Fig.

5a. A polarizer is installed on the camera so that it detects only p_x-polarized light. The sample is transparent over entire visible spectrum at normal incidence (Fig. 5b). When the incident angle is 45°, the sample is also transparent and the transmissivity is a little lower than the case at normal incidence (Fig. 5c). The sample behaves like mirror for incident angles larger than 60° (Fig. 5d). A light source is orientated towards the experimental setup. The sample looks white because most of light is reflected to the camera. We note that the sample works in air and there is no need for employing an ambient index-matching material (Supplementary Movie S1).

CONCLUSIONS

A multi-layer polymer material system that can achieve broadband angular-range selectivity over the entire visible spectrum is experimentally demonstrated. Unlike the angular-range selective films based on the Brewster angle of two *isotropic* materials, our angular-range selective film can achieve transparency around normal incidence, which enables the ambient environment to be air rather than water or any other index matching fluid. In addition, the angular-range selective film is based on a mature commercial polymer manufacturing method that can produce films at large commercial production scales. We believe that no fundamental theoretical limit exists to the angular selectivity possible while preserving broadband transmission at normal incidence. Indeed, there are several ways to narrow the angular selective window including employing a higher delta n system with increased numbers of stacks/bilayers (for example, crystalline PEN/amorphous PEN system can achieve a delta n > 0.1) Although

we only focused on p_x-polarized light in this paper (a biaxial polarization orientation will generate the same response), our method can be generalized to account for both s and p polarized light by inserting a half-wave plate (an anisotropic polymer film) between two angular selective films. [16] Such material systems could be used in many applications such as high-efficiency solar energy conversion and light trapping, privacy protection for displays, and photo-detectors with enhanced signal-to-noise ratios.

MATERIALS AND METHODS

PETG (poly ethylene terephthalate glycol) and PA (polyamide) were directly supplied from industry. Both resins were dried under vacuum at 60°C for 24 hours prior to multilayer coextrusion. Films with alternating PETG/PA layers were fabricated using a 241 layer feedblock with PA layer on the outside. Two polyethylene (PE) skin layers were added to both side of the PETG/PA multilayer core before extrusion from the exit die. The throughput of this pilot scale extrusion system was 100lbs./hr and the final films were collected in 100ft roll with 12” width.

ASSOCIATED CONTENT

Supporting Information

The Supporting Information is available free of charge at https://pubs.acs.org/doi/

Movie S1: angular selective effect movie of a rainbow picture in an iPhone screen (MP4)

ACKNOWLEDGEMENTS

This material is based upon work supported in part by the U. S. Army Research Office through the Institute for Soldier Nanotechnologies at MIT, under Collaborative Agreement Number W911NF-18-2-0048 (photon management for developing fuel-TPV mm-scale-systems). This work was also supported as a part of the S3TEC, an Energy Frontier Research Center funded by the US Department of Energy under grant no. DE-SC0001299 (for fundamental photon transport related to solar TPVs and solar-TEs). Multilayer films were extruded at Polymer Plus LLC and Rainbow Package Industrial Co., LTD. We acknowledge useful discussions with Prof. Gang Chen of MIT, Prof. John Hart of MIT, and Dr. Andrew Ouderkirk of Facebook.

COMPETING INTERESTS

Kezhen Yin, Wei Li, John D. Joannopoulos, Marin Soljačić, and Yichen Shen declare stock ownership in Lux Labs Inc.

REFERENCES

[1] Schwartz, B. T.; Piestun, R. Total External Reflection from Metamaterials with Ultralow Refractive Index. *JOSA B,* **2003,** 20 (12), 2448-2453.

[2] Alekseyev, L. V.; Narimanov, E. E.; Tumkur, T.; Li, H.; Barnakov; Y. A.; Noginov, M. A. Uniaxial Epsilon-Near-Zero Metamaterial for Angular Filtering and Polarization Control. *Applied Physics Letters,* **2010,** *97* (13), 131107.

[3] Qian, Q.; Xu, C.; Wang, C. All-Dielectric Polarization-Independent Optical Angular Filter. *Scientific Reports,* **2017,** *7* (1), 1-7.

[4] Üpping, J.; Miclea, P. T.; Wehrspohn, R. B.; Baumgarten, T.; Greulich-Weber, S. Direction-Selective Optical Transmission of 3D Fcc Photonic Crystals in the Microwave Regime. Photonics and *Nanostructures-Fundamentals and Applications,* **2010,** *8* (2), 102-106.

[5] Alu, A.; D'Aguanno, G.; Mattiucci, N., Bloemer; M. J. (2011). Plasmonic Brewster Angle: Broadband Extraordinary Transmission through Optical Gratings. *Physical Review Letters,* **2011,** *106* (12), 123902.

[6] Aközbek, N.; Mattiucci, N.; De Ceglia, D.; Trimm, R.; Alù, A.; D'Aguanno, G.; Vincenti, M. A.; Scalora, M.; Bloemer, M. J. Experimental Demonstration of Plasmonic Brewster Angle Extraordinary Transmission through Extreme Subwavelength Slit Arrays in the Microwave. *Physical Review B,* **2012,** *85* (20), 205430.

[7] Winker, B. K.; Taber, D. B. Staggered Waveplate LCD Privacy Screen. US6239853B1, 2001.

[8] Atwater, J. H.; Spinelli, P.; Kosten, E.; Parsons, J.; Van Lare, C.; Van de Groep, J.; Garcia de Abajo, J.; Polman, A,; Atwater, H. Microphotonic Parabolic Light Directors Fabricated by Two-Photon Lithography. *Applied Physics Letters,* **2011.** *99* (15), 151113.

[9] Kosten, E. D.; Kayes, B. M.; Atwater, H. A. Experimental Demonstration of Enhanced Photon Recycling in Angle-Restricted GaAs Solar Cells. *Energy & Environmental Science,* 2014, *7* (6), 1907-1912.

[10] Kosten, E. D.; Atwater, J. H.; Parsons, J.; Polman, A., Atwater, H. A. Highly Efficient GaAs Solar Cells by Limiting Light Emission Angle. *Light: Science & Applications,* 2013, *2* (1), e45.

[11] Höhn, O.; Peters, M.; Ulbrich, C.; Hoffmann, A.; Schwarz, U. T.; Bläsi, B. Optimization of Angularly Selective Photonic Filters for Concentrator Photovoltaic. In *Photonics for Solar Energy Systems IV*, *International Society for Optics and Photonics*, Brussels, Belgium, May,

2012; Vol. 8438, pp. 84380A.

[12] Shen, Y.; Hsu, C. W.; Yeng, Y. X.; Joannopoulos, J. D.; Soljačić, M. Broadband Angular Selectivity of Light at the Nanoscale: Progress, Applications, and Outlook. *Applied Physics Reviews,* **2016,** *3* (1), 011103.

[13] Clarke, G. M.; Graham, P. D.; Hansen, B. R.; Hoium, T. B.; Slama, D. F. Privacy Film. US7467873B2, 2008.

[14] MacMASTER, S. W. Privacy Screen for a Display. US7052746B2, 2006.

[15] Shen, Y.; Ye, D.; Celanovic, I.; Johnson, S. G.; Joannopoulos, J. D.; Soljačić, M. Optical Broadband Angular Selectivity. *Science,* **2014,** *343* (6178), 1499-1501.

[16] Qu, Y.; Shen, Y.; Yin, K.; Yang, Y.; Li, Q.; Qiu, M.; Soljačić, M. Polarization-Independent Optical Broadband Angular Selectivity. *ACS Photonics,* **2018,** *5* (10), 4125-4131.

[17] Hamam, R. E.; Celanovic, I.; Soljačić, M. Angular Photonic Band Gap. *Physical Review A,* **2011,** *83* (3), 035806.

[18] Liu, V.; Fan, S. S4: A Free Electromagnetic Solver for Layered Periodic Structures. *Computer Physics Communications,* **2012,** *183* (10), 2233-2244.

[19] Ponting, M.; Hiltner, A.; Baer, E. Polymer Nanostructures by Forced Assembly: Process, Structure, and Properties. *Macromol. Symp.* **2010,** *294-I,* 19.

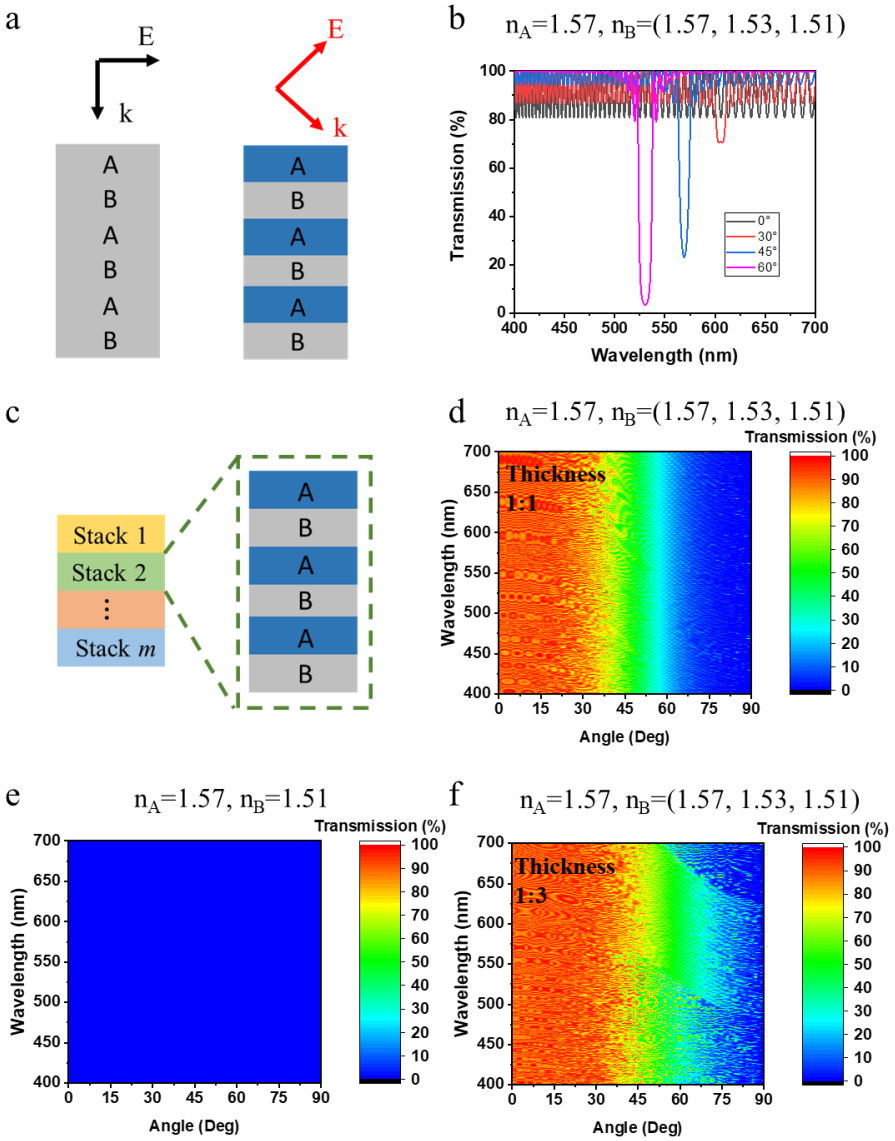

Fig 1. | Theoretical illustration. a, Schematic diagrams showing p_x-polarized light incident at zero and nonzero angles on 1D PhC. Different colors (blue and grey) represent different refractive indices of bilayers. Band gaps only appear at nonzero incident angles. **b,** Transmission spectra for p_x-polarized light incident at zero and nonzero angles on 1D PhC. 1D PhC has 80 bilayers and the period is 100 nm. **c,** Schematic layout of the bilayer structure stacking mechanism. **d,** p_x-polarized transmission spectrum of 85 stacks at various periodicities. Each stack consisting of 50 isotropic-anisotropic bilayers. The thickness ratio between layer A and B is 1:1. **e,** p_x-polarized transmission spectrum of isotropic-isotropic 1D PhC stacks. There are 1000 stacks, 50 isotropic-anisotropic bilayers in each stack. This system behaves like a mirror at any incident angle and visible wavelength, thus emphasizing the importance of the need to introduce anisotropy. **f,** p_x-polarized transmission spectrum of 85 stacks, 50 isotropic-anisotropic bilayers in each stack. The thickness ratio between layer A and B is 1:3.

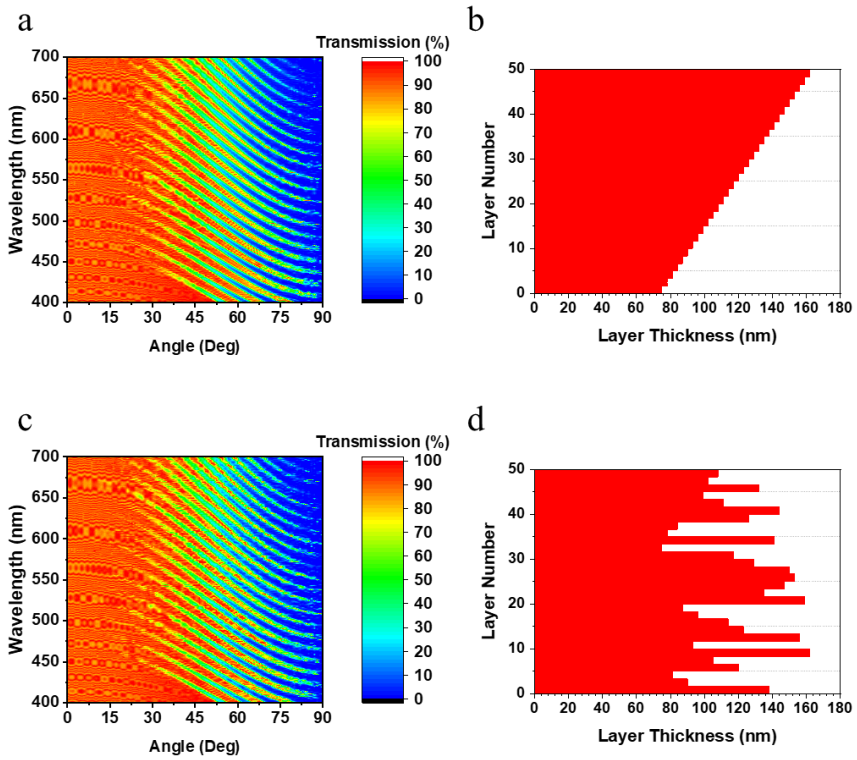

Fig 2. | Spectra of sequentially and randomly distributed multilayer structures. a, p_x-polarized transmission spectrum of 30 stacks at various periodicities. Each stack consisting of 100 isotropic-anisotropic bilayers. **b,** The sequential thickness distribution of 30 stacks ranging from 70 nm to 160 nm with a step of 3 nm. **c,** p_x-polarized transmission spectrum of 30 stacks with a random distribution. **d,** The random thickness distribution of 30 stacks ranging from 70 nm to 160 nm.

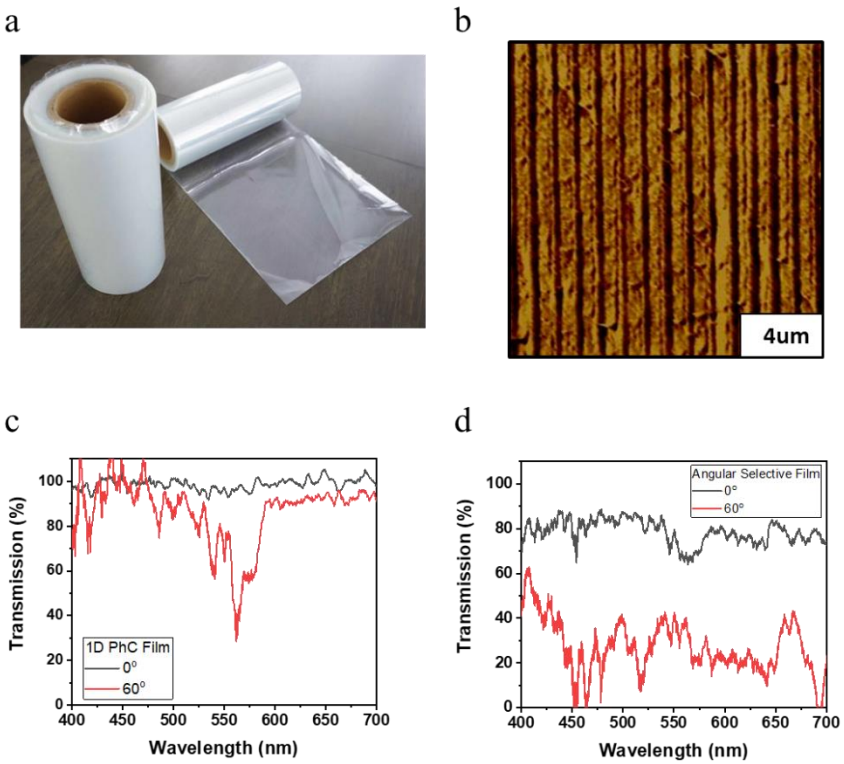

Fig. 3 | Experimental samples and measured spectra. **a,** Continuous fabrication of multilayer films. Film width = 30 cm; film length = 100 m. **b,** AFM phase image of angular selective film cross section. **c,** p_x-polarization transmission spectrum of 1D PhC film at 0° (transparent) and 60° (bandgap). **d,** p_x-polarization transmission spectrum of angular selective film with 20 of 1D PhC stacks at 0° (~80% average transmissivity) and 60° (~25% average transmissivity).

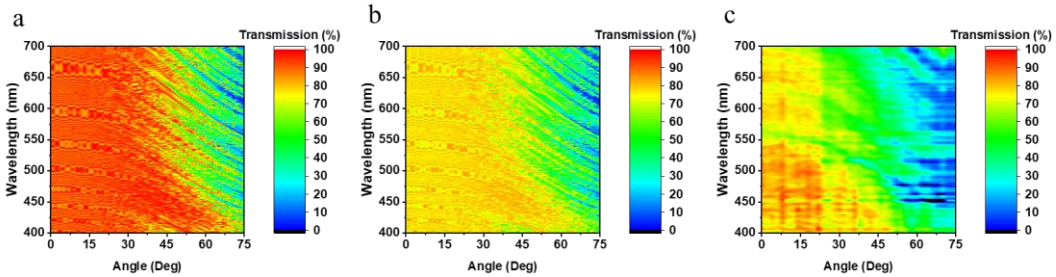

Fig. 4 | Calculated and measured spectra. The calculated transmission spectra for p_x-polarized light a, without scattering correction and **b,** with scattering correction. **c,** The experimental transmission spectra for p_x-polarized light. The value of transmission is indicated by the color bars.

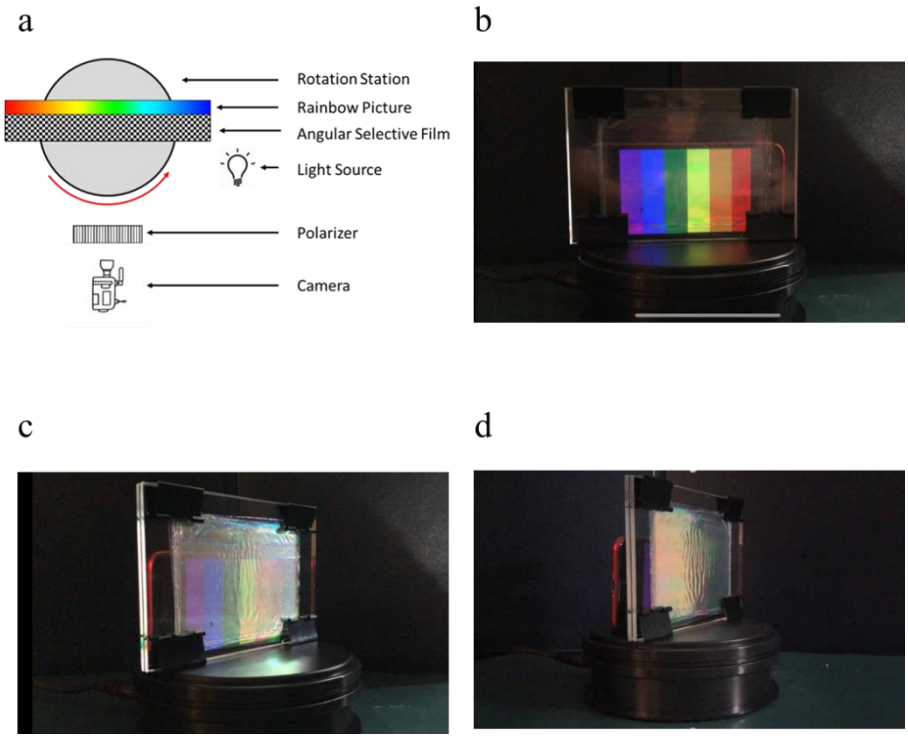

Fig 5. | Experimental setup and observations. a, Schematic of experiment setup. The rainbow picture and angular selective film are installed on a rotation station. A polarizer is placed in front of a camera. Large scale result on iPhone: **b,** Incident angle is 0°. The angular selective film is transparent for the entire visible regime for p_x-polarized light. **c,** Incident angle is 45°. The transmissivity of the angular selective film is decreased a little. **d,** Incident angle is 60°. The angular selective film behaves as a mirror.

For Table of Contents Only